Influence of Lysine N^{ε}-Trimethylation and Lipid Composition on the Membrane Activity of the Cecropin A-Melittin Hybrid Peptide CA(1−7)M(2−9)†

Vitor Teixeira,[‡,§] Maria J. Feio,[§] Luis Rivas,[||] Beatriz G. De la Torre,[⊥] David Andreu,[⊥] Ana Coutinho,[#] and Margarida Bastos*[,‡]

CIQ (UP) Department of Chemistry and Biochemistry, Faculty of Sciences, University of Porto, P-4169-007 Porto, Portugal, REQUIMTE, Faculty of Sciences, University of Porto, P-4169-007 Porto, Portugal, Centro de Investigaciones Biologicas (CSIC), lab#300, Ramiro de Maeztu, 9 E-28040-Madrid, Spain, Department of Experimental and Health Sciences, Pompeu Fabra University, E-08003 barcelona, Spain, and CQFM and IN, Instituto Superior Técnico, UTL, P-1049-001 Lisbon, Portugal

Received: July 24, 2010; Revised Manuscript Received: September 1, 2010

Although many studies have pointed out the promising role of antimicrobial peptides (AMPs) as therapeutical agents, their translation into clinical research is being slow due to the limitations intrinsic to their peptide nature. A number of structural modifications to overcome this problem have been proposed, leading to enhanced AMP biological lifetimes and therapeutic index. In this work, the interaction between liposomes of different lipidic composition and a set of lysine N^{ε}-trimethylated analogs of the cecropin A and melittin hybrid peptide, CA(1−7)M(2−9) [H-KWKLFKKIGAVLKVL-amide], was studied by differential scanning calorimetry (DSC) and fluorescence spectroscopy. The study was carried out using membrane models for mammalian erythrocytes (zwitterionic lipids) and for bacteria (mixture of zwitterionic and negatively charged lipids). The results show that trimethylated peptides interact strongly with negatively charged (bacterial cell model) but not with zwitterionic (erythrocyte model) liposomes. These results are in agreement with the reduction of cytotoxicity and ensuing improvement in therapeutic index vs parental CA(1−7)M(2−9) found in a related study. Moreover, the modified peptides act differently depending on the model membrane used, providing further evidence that the lipid membrane composition has important implications on AMP membrane activity.

Introduction

In the last decades there has been an alarming increase in pathogenic microorganisms multiresistant to conventional antibiotics, often with the phenotype being reached over very short periods of time.[1−8] Thus, vancomycin-resistant enterococci (VRE) and methicillin-resistant *Staphylococcus aureus* strains (MRSA) have been reported with increasing frequency worldwide.[9] In this crisis scenario, with substantial effort devoted to the discovery of new antibiotic chemotherapeutic resources and strategies, antimicrobial peptides (AMPs) are receiving considerable attention.

AMPs are present in the defense systems of virtually all forms of life, from bacteria to plants, invertebrate and vertebrate species.[4,5,7,8,10−17] They take part on both innate and adaptive immune responses by mounting a first line of defense against pathogens and producing a diverse range of immunomodulatory effects through a variety of mechanisms at different levels.[18,19] Most AMPs are 12−50 amino acids long and contain 1−9 positively charged lysine or arginine residues, essential for activity.[7,8,13,20] A correspondingly sizable proportion of hydrophobic residues allow AMPs to adopt amphipathic conformations.

Different mechanisms of action for AMPs have been reported, which involve membrane permeabilization through the formation of stable pores (either barrel-stave or toroidal pore's type), membrane thinning (molecular electroporation or sinking rafts models), or micellization of the membrane in a detergent-like action (carpet model).[21] More recently, the association of α-helices into amyloid fibril-like supramolecular entities has been progressively demonstrated, with transversal implications both on the mechanism of action and immune properties of some antimicrobial peptides, such as temporins B and L[22] and dermaseptins,[23] and on the paradigm of lipid-binding properties and action of amyloid-forming cytotoxic peptides[24,25] [e.g., amyloid β-protein (Aβ)], responsible for many neurodegenerative disorders (Alzheimer's disease, Parkinson disease and transmissible spongiform encephalopathies). Therefore, the leakage of ions and other metabolites, loss of cytoplasmic components, dissipation of electrochemical potentials and ultimately cell death, are some of the reported sequential events on the basis of their microbicidal action toward pathogens. Moreover, AMPs may translocate across the membrane and affect cell metabolism by modulating particular core metabolic pathways after gaining access to intracellular targets, such as DNA, enzymes and even organelles (mitochondria). More recently, these peptides have been shown to produce significant membrane perturbation by lateral phase segregation of zwitterionic from anionic phospholipids,[26] the induction of nonlamellar phases at physiologically relevant conditions[27,28] and in some cases the formation of specific lipid−peptide interactions.[29]

Most AMPs usually display a broad range activity by acting on bacteria, fungi, parasites, viruses, and even cancer cells.[26] AMPs achieve specific permeabilization by exploiting the large

† Part of the "Robert A. Alberty Festschrift".

* Corresponding author. E-mail: mbastos@fc.up.pt. Tel: + 351 22 0402511. Fax: +351 22 0402659.

‡ CIQ (UP) Department of Chemistry and Biochemistry, University of Porto.

§ REQUIMTE, University of Porto.

|| Centro de Investigaciones Biologicas (CSIC).

⊥ Pompeu Fabra University.

Instituto Superior Técnico.

10.1021/jp106915c
Published on Web 10/12/2010

TABLE 1: Amino Acid Sequences of the Parental Hybrid Peptide CA(1−7)M(2−9) and its N$^{\epsilon}$-Trimethylated Derivatives K6 and K7

peptide	sequence
CA(1−7)M(2−9)	KWKLFKKIGAVLKVL-amide
K6	KWKLF**K**(Me)$_3$KIGAVLKVL-amide
K7	KWKLFK**K**(Me)$_3$IGAVLKVL-amide

difference between prokaryotic and eukaryotic cells with regards to plasma membrane lipid composition,[21] a factor therefore essential in designing realistic model membranes from which valid information on AMP effectiveness can be drawn. Phosphatidylcholine (PC) and phosphatidylethanolamine (PE) are typically used as zwitterionic lipids on model membranes. In particular, PE can represent 75% to 80% of the lipid membrane composition of bacteria, as observed for *Escherichia coli*, along with anionic phospholipids (phosphatidylglycerol and cardiolipin).[30] On the other hand, the usual mammalian model system, the erythrocyte, is mainly composed of zwitterionic lipids (phosphatidylcholine, sphingomyelin, and cholesterol).[31]

There is widespread acceptance that the initial mechanism by which AMPs target membranes is mediated by an electrostatic interaction of the cationic peptides to the negatively charged membranes, accounting for the membranotropism of AMPs toward pathogens.[1,5,7,8,11,17] As a consequence, they have not been very successful in counteracting the action of AMPs since that would require an overall reorganization of the cell membrane structure or phospholipid composition.

To counteract the limitations inherent to most peptide pharmaceuticals, a number of modifications enhancing AMP activity and reducing cytotoxicity have been proposed.[32−37] In this work we examine one such modification, namely Lys N$^{\epsilon}$-trimethylation, which despite its substantial role in epigenetics, has only recently received attention as a promising way to rationally improve key pharmacokinetic parameters and bioavailability, as observed for cyclosporine and cyclopeptidic somatostatin analogues.[38,39]

The effect of Lys N$^{\epsilon}$-trimethylation at selected positions was examined using a well-known AMP platform, the cecropin A-melittin hybrid peptide CA(1−7)M(2−9) [H-KWKLFKKIGAVLKVL-amide].[40] We have performed a series of biophysical studies on the most promising analogs, in an attempt to understand the mechanism by which trimethylation increases the therapeutical index and evaluate the effect of this modification on the peptide's activity. Two Lys-trimethylated derivatives (K6 and K7) were initially evaluated by DSC and fluorescence spectroscopy on large unilamellar vesicles (LUVs) made of mixtures of 1,2-dimyristoyl-*sn*-glycero-3-phosphocholine (DMPC) and 1,2-dimyristoyl-*sn*-glycero-3-phospho-(1′-*rac*-glycerol) (DMPG), namely, DMPC:DMPG (3:1), as it was the membrane system previously used to study the parental peptide CA(1−7)-M(2−9).[41,42] In addition, the interaction with another bacterial membrane model, LUVs of 1-palmitoyl-2-oleoyl-*sn*-glycero-3-phosphoethanolamine (POPE) and 1-palmitoyl-2-oleoyl-*sn*-glycero-3-phospho-(1′-*rac*-glycerol) (POPG), POPE:POPG (3:1), was also studied to ascertain the dependence of activity on lipid composition. The partition of the trimethylated peptides to DMPC vesicles was also evaluated to appraise their cytotoxicity toward mammalian cell membranes.

Experimental Section

Materials. 1,2-Dimyristoyl-*sn*-glycero-3-phosphocholine (DMPC), 1,2-dimyristoyl-*sn*-glycero-3-phospho-*rac*-(1-glycerol) (DMPG), 1-palmitoyl-2-oleoyl-*sn*-glycero-3-phosphoethanolamine (POPE), 1-palmitoyl-2-oleoyl-*sn*-glycero-3-phospho-(1′-*rac*-glycerol) (POPG) lipids were obtained from Avanti Polar Lipids (Alabaster, AL) and used without further purification.

Reagents and resins, as well as protocols for the solid phase synthesis of CA(1−7)M(2−9) and its Lys N$^{\epsilon}$-trimethylated analogs have been recently reported.[40]

HEPES buffer [(*N*-(2-hydroxyethyl)piperazine-*N*9-ethanesulfonic acid) (Sigma), NaCl (Merck) and ultra pure water (Milli Q Gradient, Millipore, Billerica, MA), were used to prepare the buffer as solvent (10 mM, 100 mM NaCl, pH 7.4). Peptide stock solutions were prepared from powder in the same buffer and quantified by either amino acid analysis or ultraviolet absorption at 280 nm, taking 5690 $M^{-1}\cdot cm^{-1}$ as the molar extinction coefficient corresponding to the single tryptophan residue present in the studied peptides.[42,43]

Vesicle Preparation. Appropriate amounts of phospholipids were dissolved in chloroform (DMPC) or chloroform/methanol (3:1 v:v) [(POPE:POPG (3:1) and DMPC:DMPG (3:1)]. The samples were dried under a slow nitrogen stream, and the film was kept under vacuum and protected from light for three hours to remove all traces of organic solvents. The resulting lipid film was warmed together with HEPES buffer (10 mM HEPES, 100 mM NaCl, pH 7.4) for about 1 h in a thermostated water bath at approximately 10 °C above the temperature of the gel-to-liquid crystalline phase transition (T_M) to guarantee that the lipid system is at the fluid phase. The lipid vesicles thus obtained were frozen in liquid nitrogen and thawed in the thermostated bath, and this process was repeated 5 times. Large unilamellar vesicles (LUVs) were obtained from the original MLVs by extrusion in a 10 mL stainless steel extruder (Lipex Biomembranes, Vancouver, British Columbia, Canada), thermostated with a circulating water bath at 10 °C above T_M. The lipid suspensions were passed several times through polycarbonate filters (Nucleopore, Pleasanton, CA) of decreasing pore size (600, 200, and 100 nm, 5, 5, and 10 times, respectively), under inert (N_2) atmosphere and pressure. Size distribution of the extruded vesicles was determined by dynamic light scattering (ZetaSizer NanoZS, Malvern Instruments, Malvern, Worcestershire, U.K.) at 37 °C, using a He−Ne laser (wavelength 633 nm) as a source of incident light, and operating at a scattering angle of 173°. Mean particle size was determined to be 112 ± 14 nm (average and standard deviation of six independent measurements).

Steady-State Fluorescence Spectroscopy. Stock solutions (6 mM) of DMPC and DMPC:DMPG (3:1) LUVs were prepared as above. Unless otherwise stated, the concentration of the peptide solutions in the same buffer was 10 μM. Addition of appropriate aliquots of liposome suspension into the peptide solution was performed so as to cover a range of liposome concentrations (0−500 μM). Independent measurements were performed for the pure peptide solution and at increasing liposome concentration. The mixtures were prepared and allowed to equilibrate at 37 °C for 30 min before measurements. All measurements were performed at this temperature.

The measurements were performed on a Varian Cary Eclipse spectrofluorometer (Varian Inc., Palo Alto, CA) equipped with a multicell sample holder and a temperature control unit. Samples were excited at 280 nm with emission spectra collected in the 300−450 nm wavelength range. The scanning rate was 1 nm/min and slit widths of 5 nm were used for both the excitation and emission settings. Several spectra were recorded consecutively and averaged in the final analysis.

Steady-state fluorescence anisotropy measurements were recorded with a SLM-8000C spectrofluorometer using cells with

5 mm path length. For all experiments, the sample absorbance at 280 nm was <0.05. For the anisotropy determination, the corresponding vertically and horizontally polarized emission intensities, elicited by vertically and horizontally polarized excitation using Glan-Thompson polarizers, were corrected for background contribution.[44] The lipid concentration was low enough to prevent a significant light scattering from the suspension that could result in an artificial depolarization of the fluorescence.

Time-Resolved Fluorescence Spectroscopy (TRFS). Stock solutions (6 mM) of POPE:POPG (3:1) LUVs were prepared as above and used in these measurements. Unless otherwise stated, the concentration of the peptide solutions in the same buffer was 10 μM. Independent measurements were performed for the pure peptide solution and at increasing liposome concentration between 0 and 2000 μM. The mixtures were prepared and allowed to equilibrate at 30 °C for 30 min before measurements. The sample was excited at 282 nm using a frequency doubled, cavity dumped (3.7 MHz repetition rate), dye laser of rhodamine 6G (Coherent (Santa Clara, CA) 701-2), synchronously pumped by a mode-locked Ar laser (514.5 nm, Coherent Innova 400-10). The emission was detected by a Hamamatsu (Bridgewater, NJ) R-2809 MCP photomultiplier at 350 nm (Jobin-Yvon (Edison, NJ) HR320 monochromator). The instrument response functions were generated from a scattering particle dispersion (silica, colloidal water suspension, Aldrich, Milwaukee, WI). The time scaling was 11 ps per channel, and 1024 channels were in use. Data analysis was carried out using a nonlinear least-squares iterative method based on the Marquardt algorithm. The goodness of fit was judged from the obtained χ^2 values (a value of $\chi^2 \leq 1.3$ was considered acceptable), random distribution of weighted residuals, and autocorrelation plots.

The complex decay of tryptophan was described by a sum of exponentials:[42]

$$I(t) = \sum_{i=1}^{n} \alpha_i e^{-t/\tau_1} \tag{1}$$

where α_i and τ_i are the normalized amplitude and the lifetime of the ith decay component, respectively. From the fluorescence intensity decay kinetics of the Trp residue, the amplitude-weighted mean fluorescence lifetime, $\bar{\tau}$ (also called the lifetime-weighted quantum yield) was calculated as

$$\bar{\tau} = \sum_{i=1}^{n} \alpha_i \tau_i \tag{2}$$

To study the rotational and segmental dynamics of the peptide's tryptophan residues, time-resolved fluorescence anisotropy decay measurements were also carried out under identical conditions aforementioned, both in buffer solution and upon peptide binding to liposomes.[44] An excitation wavelength of 300 nm instead of 282 nm was used because the fundamental anisotropy of the indole chromophore in a glass state reaches its highest value ($r_0 \sim 0.3$) at this wavelength.[45]

Determination of Partition Constants. The association of the peptides (P) to the model membranes can be described quantitatively in terms of simple partition equilibrium between the aqueous (W) and the lipid bilayer phase (L):[42]

$$K_{p,x} = \frac{\dfrac{n_L^P}{n_L + n_L^P}}{\dfrac{n_W^P}{n_W + n_W^P}} \tag{3}$$

where $K_{p,x}$ represents the mole-fraction partition constant of the peptide, n_W and n_L are the amount (in mol) of water and lipid in each sample, respectively, and n_i^P is the amount of peptide present in each phase (i = W, aqueous phase, and i = L, lipid phase, respectively). In all partitioning experiments, it is reasonable to assume that $n_w \gg n_w^P$, and because high membrane-bound concentrations of the peptide are usually avoided to prevent deviations from ideal partitioning due to peptide/peptide interactions at the water:membrane surface or in the lipid bilayer, it can also be considered that $n_L \gg n_L^P$. Therefore, eq 3 can be simplified to a still dimentionless $K_{p,x}$ as

$$K_{p,x} = \frac{\dfrac{n_L^P}{n_L}}{\dfrac{n_W^P}{n_W}} \tag{4}$$

If the amounts of lipid and water are replaced by their respective molar volumes, the Nernst partition constant is obtained (K_p), which is related to the previous one according to eq 5:[46]

$$K_{p,x} = K_p \times \frac{\gamma_L}{\gamma_W} \tag{5}$$

where γ_L and γ_W correspond to the molar volume of lipid and water, respectively. In the present study, the mole-fraction partition constant was used throughout.

Fluorescence data were analyzed by use of the formalism above. In the case of TRFS eq 6 was used to relate the lifetime-weighted quantum yield, $\bar{\tau}$, to the mole-fraction partition constant $K_{p,x}$:[42]

$$\bar{\tau} = \frac{\bar{\tau}_W + K_{p,x} \times \gamma_W \times |L| \times \bar{\tau}_L}{1 + K_{p,x} \times \gamma_W \times |L|} \tag{6}$$

where $\bar{\tau}_W$ and $\bar{\tau}_L$ stand for the lifetime-weighted quantum yield in the aqueous phase (buffer) and in the lipid phase and |L| stands for the lipid concentration on the outer leaflet. This equation was fitted to experimental data of $\bar{\tau}$ versus lipid concentration, to obtain the mole-fraction partition constant ($K_{p,x}$) and the lifetime-weighted quantum yield in the lipid phase, $\bar{\tau}_L$.

For steady-state fluorescence spectroscopy partitioning experiments the data was also initially analyzed according to a simple partition model by means of eq 7:[46]

$$\Delta I = \frac{\Delta I_{max} \times K_{p,x} \times |L|}{|W| + K_{p,x} \times |L|} \tag{7}$$

where $\Delta I = I - I_o$ stands for the difference between the steady-state fluorescence intensity of the peptide measured in the presence (I) and in the absence of phospholipid vesicles (I_o);

$\Delta I_{max} = I_\infty - I_o$ is the maximum value of this difference, since I_∞ is the limiting value of I measured upon increasing the lipid concentration, |L| is the lipid concentration on the outer leaflet, and $K_{p,x}$ is the mole-fraction partition constant of the peptide between the aqueous and lipid phases. The parameter |W| is the molar concentration of water (55.3 M at 37 °C).[46]

Differential Scanning Calorimetry (DSC). The experiments were performed in a Micro-DSC III, SETARAM (Caluire, France) and in a VP-DSC (MicroCal, LLC, Northampton, MA). Two or more successive up and down scans were performed for each sample, all at a scanning rate of 1 °C·min^{-1}, over the temperature range 5−45 °C. The sample mixtures were prepared immediately before the DSC run, by adding the desired amount of peptide stock solution to the LUVs suspension [DMPC:DMPG (3:1) and POPE:POPG (3:1)]. The measurements for the first lipid system were performed in the Setaram Micro-DSCIII and the last system in the VP-DSC. All procedures regarding handling (lag time at low temperature, time between mixture and start of the experiment) were kept constant, to ensure that all samples had the same thermal history. Both instruments were electrically calibrated for temperature and scan rate, either by ourselves (MicroDSC III) or by the company (VP-DSC). The respective data treatment software was used for baseline subtraction and calculation of the gel-to-liquid crystalline phase transition thermodynamic parameters, namely transition temperature (T_M) and enthalpy (ΔH). For consistency and comparability of all experiments, the integration was always performed between the two points where the curves start to deviate from and return to the baseline. A linear baseline was considered between the initial and final integration temperatures.

Results

Energetics of the Peptide−Membrane Binding Equilibrium by DSC. The specificity and affinity of the peptide toward lipid mixtures were evaluated through their effect on the thermodynamic parameters of the liposome's thermotropic phase transition.[47,48] The characterization here used is based on the gel-to-liquid crystalline phase transition temperature (T_M) and the corresponding enthalpy change (ΔH). For each lipid system, series of measurements were done using the same liposome preparation, at different P:L ratios, and within 5 days, for all differences found to be ascribed to the peptide action and not to intersample variation or sample deterioration.

Figure 1 shows the DSC curves of pure DMPC:DMPG (3:1) vesicles and the influence of the peptide on the thermotropic transition for different P:L ratios.

The thermodynamic parameters obtained for the pure lipid system (T_M = 25.3 °C and ΔH = 26 kJ/mol) are in very good agreement with the literature.[41] The overall effect of K6 and K7 peptides on the main thermotropic phase transition is characterized by a modest shift to lower temperatures at low P:L ratios, and marginal changes on the transition enthalpy (Table 2), similarly to what was observed for CA(1−7)M(2−9) by Abrunhosa et al.[41] Nevertheless, for the K7 peptide at P:L = 1:80 we already observe a peak splitting with one peak at lower (24.8 °C) and another at higher (28.0 °C) temperature than the one for the pure lipid system. This behavior has been ascribed to preferential binding of the peptide to the negatively charged lipids, leading to their segregation within the membrane.[47−50] At the highest P:L ratio (1:15), the change in ΔH is much more significant for the K7 derivative (a reduction of 38% of the pure lipid enthalpy change) as compared to that of the other methylated analogue and of the parental peptide CA(1−7)-M(2−9).[41] At this higher ratio, a peak splitting is now also observed for K6 derivative (Table 2). It is interesting to note that CA(1−7)M(2−9) only presents a profile consistent with modest lipid segregation at P:L ratio 1:40, whereas at 1:15 massive destruction and a totally distorted profile is observed.[41]

Moreover, the cooperativity also decreased in all cases (Figure 1), judging by the increase of the half-height width. At low

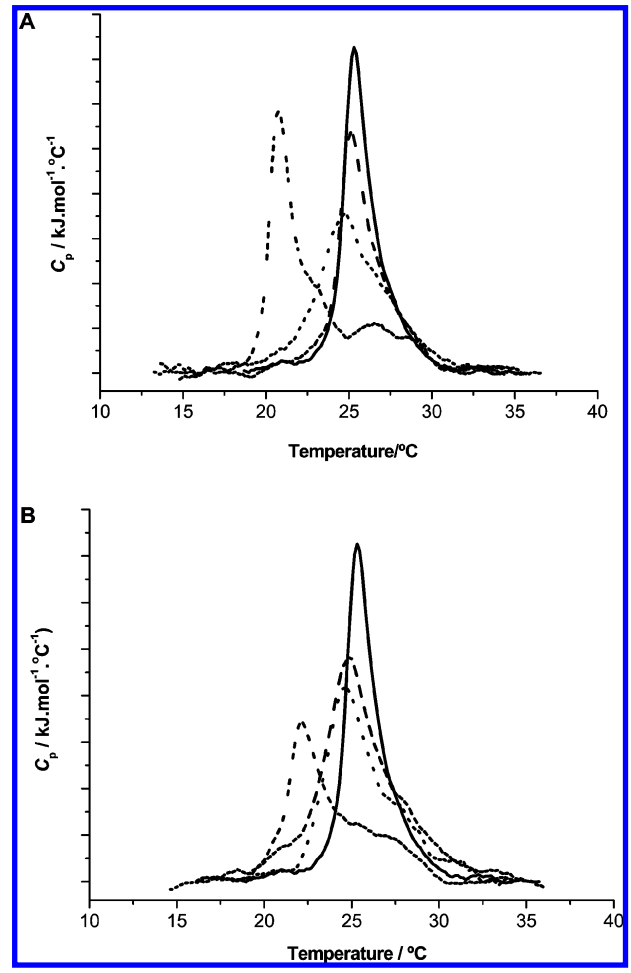

Figure 1. DSC thermograms for peptide and DMPC:DMPG (3:1) lipid systems at different P:L ratios for the trimethylated versions K6 (A) and K7 (B): pure lipid (solid line), 1:80 (dashed line), 1:40 (dotted line), and 1:15 (short dashed line). The lipid concentration was 3 mM in all experiments.

TABLE 2: Thermodynamic Parameters for the Interaction of the Trimethylated Analogues K6 and K7 for the Lipid System DMPC:DMPG (3:1) As Obtained by DSC[a]

peptide	P:L molar ratio	T_M (°C)	ΔH (kJ·mol^{-1})
CA(1−7)M(2−9)[b]	0	26.2	28
	1:80	26.3	28
	1:40	25.5	28
	1:15	21.3	22
K6	0	25.3	26
	1:80	25.1	23
	1:40	24.9	22
	1:15	20.8/26.8	24
K7	0	25.3	26
	1:80	24.8/28.0	25
	1:40	24.6/28.0	24
	1:15	22.1/27.4	16

[a] The estimated uncertainly in T_M is ±0.3 °C and in ΔH is ±1 kJ·mol^{-1}; P:L ratio stands for molar ratio. [b] Values obtained from Abrunhosa et al.[41]

P:L ratio, the symmetry of the peak is still kept, suggesting the perturbation was small, probably resulting from an interaction of the peptide with the phospholipid headgroups, at the water/membrane interface.[50] Upon an increase of peptide concentration, the perturbation becomes more pronounced due to the dominant role of the electrostatic interaction between the negatively charged phospholipids and the highly cationic peptide.

The interaction of both parental and trimethylated derivatives was also studied using another bacterial mimetic system, namely, POPE:POPG (3:1) to unearth the activity dependence on the lipid composition.

Figure 2 shows the DSC curves of pure POPE:POPG (3:1) vesicles for the same P:L ratios tested for the DMPC:DMPG (3:1) model system. The transition temperature and enthalpy change for the pure lipid system is in good agreement with previous studies for a similar POPE:POPG ratio.[51]

At low peptide-to-lipid ratios (1:80), both CA(1−7)M(2−9) and K6 show an increase in both transition temperature and enthalpy, consistent with a stabilization of the gel phase ($L\beta'$) (Figure 2). This type of stabilizing effect has been reported by Schwieger et al. for the binding of poly(L-lysine) to DPPG membranes.[52] Interestingly, the same effect is not observed for K7, as the thermogram for this peptide points out to lipid segregation already at this P:L ratio. This suggests that the electrostatic interaction is somehow improved with K7.

In the PE:PG system, we propose that the initial stabilizing effect is mainly due to the fact that at low peptide concentrations the partition may promote a more structured and compact lipid chain packing due to the electrostatic interaction of the peptide with both polar lipid headgroups, before significant segregation takes place.

At 1:40, all peptides led to the appearance of two peaks indicating a peptide-mediated domain segregation. The first peak at low temperature is assigned to a peptide-rich, POPG-enriched domain, and the second one, at a higher temperature, corresponds to a peptide-poor, POPE-enriched domain, consistent with the main transition temperatures of the pure lipids (Table 3). At the highest peptide-to-lipid ratio (1:15), the effect of CA(1−7)M(2−9) on the bilayer is particularly dramatic as a very pronounced decrease in the enthalpy (without peak splitting) is observed for this P:L ratio.

Partition of the Peptide to Membrane Systems As Studied by Fluorescence Spectroscopy. ***DMPC and DMPC:DMPG (3:1) Model Membranes.*** In all cases, the peptides in buffer present a fluorescence emission maximum at 350 nm, typical for Trp in a polar environment. When mixed with DMPC vesicles, the methylated peptides have no significant partition to the membrane system, since there is no shift in emission maximum, and thus the Trp environment is not altered upon increasing the lipid concentration (data not shown). The parental peptide CA(1−7)M(2−9) was studied earlier by Abrunhosa et al.[41] and Bastos et al.,[42] and it was shown to partition to DMPC vesicles. These results fully agree with hemolytic studies,[40] where the parental peptide CA(1−7)M(2−9) was found to be somewhat hemolytic whereas a pronounced decreased in hemolytic activity was observed for the monosubstituted derivatives studied here (K6 and K7).

The presence of anionic phospholipids [DMPC:DMPG (3:1)]) was accompanied by a drastic change on the partition profile—a general increase in fluorescence intensity as well as a considerable spectral shift of about 15 nm to lower wavelengths (data not shown) ensued, evidencing the insertion of Trp residues into a more hydrophobic environment upon increasing the lipid concentration. The intensity differences ΔI (see Experimental Section) are plotted against the lipid concentration (outer leaflet) in Figure 3.

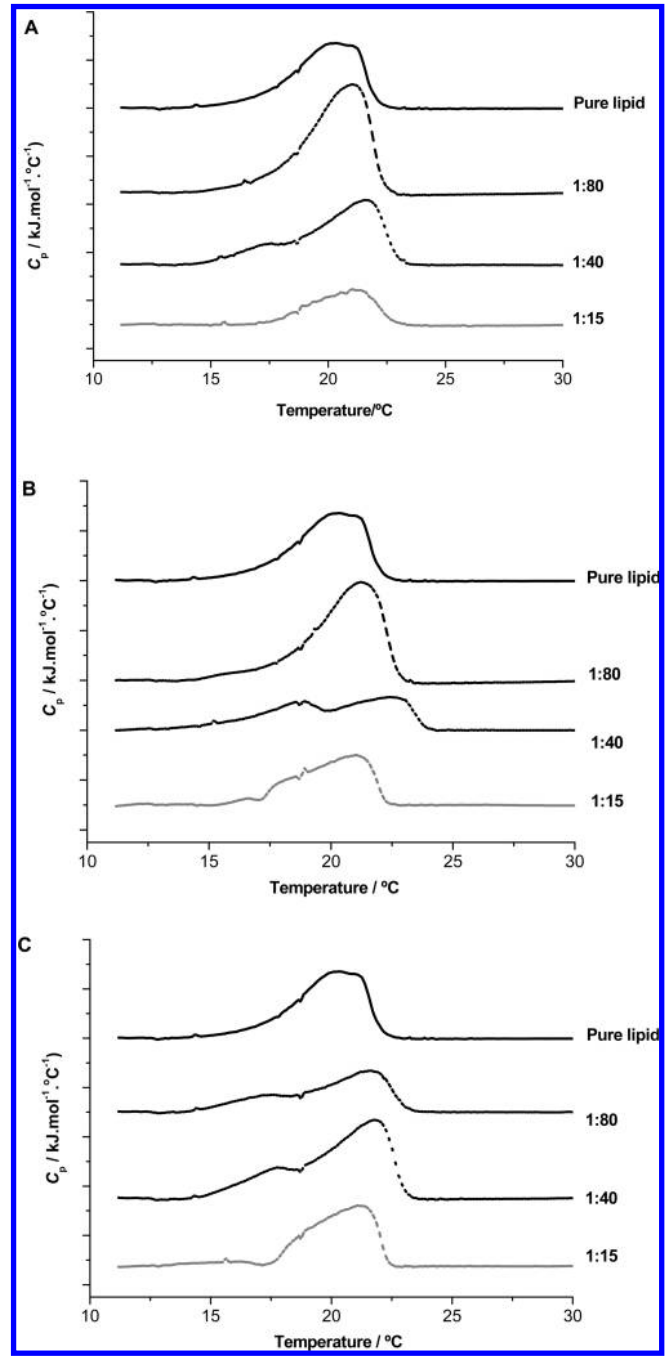

Figure 2. DSC thermograms for pure lipid system, POPE:POPG (3:1) at different P:L ratios (1:80, 1:40, and 1:15) for the parental peptide CA(1−7)M(2−9) (A) and the trimethylated versions K6 (B) and K7 (C): pure lipid (solid line), 1:80 (dashed line), 1:40 (dotted line) and 1:15 (gray short dashed line). The lipid concentration was 2 mM in all experiments.

As can be seen, the increase in intensity follows a simple partition model (eq 7) in the initial and final stages of the partition, whereas a sharp maximum is apparent for P:L ratio 1:9, with the intensity returning to the expected values for simple partition soon after (Figure 3). This behavior is consistent with membrane saturation, as already observed by Bastos et al.[42] for the parental peptide CA(1−7)M(2−9) and Melo et al.[53] for omiganan peptide. It can be interpreted as a result of the

TABLE 3: Thermodynamic Parameters for the Interaction of CA(1−7)M(2−9) and the Trimethylated Analogues K6 and K7 for the Lipid System POPE:POPG (3:1) As Obtained by DSC[a]

peptide	P:L molar ratio	T_M (°C)	ΔH (kJ·mol^{-1})
CA(1−7)M(2−9)	0	20.4	22
	1:80	21.2	33
	1:40	17.2/21.5	27
	1:15	21.1	12
K6	0	20.4	22
	1:80	21.3	32
	1:40	17.7/22.7	17
	1:15	18.6/21.1	16
K7	0	20.4	22
	1:80	17.2/21.7	17
	1:40	17.8/21.8	30
	1:15	15.1/21.1	20

[a] The estimated uncertainty in T_M is ±0.3 °C and in ΔH is ±1 kJ·mol^{-1}; P:L ratio stands for molar ratio.

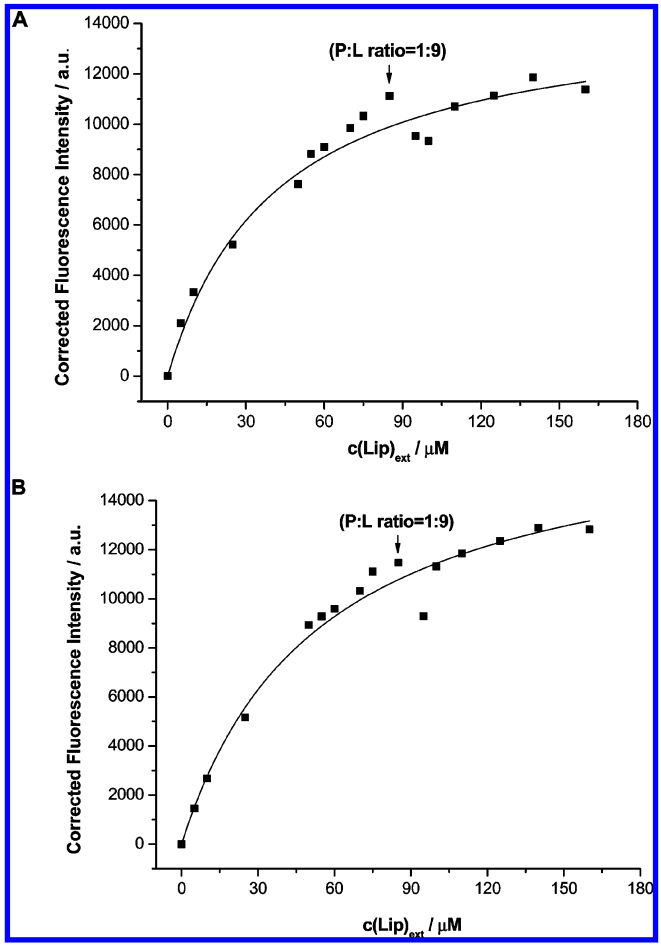

Figure 3. Representation of steady-state fluorescence intensity differences, ΔI, as a function of the lipid concentration (outer leaflet) for the DMPC:DMPG (3:1) system at 37 °C. The symbol (■) represents the experimental values, and the line corresponds to the fitted curve according to eq 7 for the trimethylated versions K6 (A) and K7 (B) (see Experimental Section). The excitation and emission wavelength range were 280 and 300−450 nm, respectively.

dominant role of the electrostatic interaction between the anionic headgroups of the phospholipids and the highly positively charged peptide (nominal net charge +6 at physiological conditions) at low lipid concentrations, which is reflected by a high initial slope in the partition curve and a sharp maximum in intensity. This maximum would thus represent membrane saturation and we propose it to be related to membrane charge neutralization. Despite the presence of this maximum, we can see in Figure 3 that overall a simple partition model can be fitted to the obtained data. $K_{p,x}$ values were extracted by fitting all points except for the increase in the maxima and the sharp saturation regime (it was considered the five leftmost and the four rightmost experimental points) using eq 7. The $K_{p,x}$ values so obtained were $(1.3 \pm 0.2) \times 10^6$ and $(1.0 \pm 0.1) \times 10^6$, for K6 and K7 derivatives, respectively. Interestingly, CA(1−7)-M(2−9) was also found to present a lower threshold value (P:L ratio 1:12) according to TRFS studies performed to extract the partition constant.[42] For this peptide, K_p estimates were previously provided[42] that we converted to $K_{p,x}$ values according to eq 5, leading to 3.2×10^6 and 3.9×10^6, depending on the curve region used to get the estimate. Even considering that the previous values for the parental peptide were estimates, it can be seen that the $K_{p,x}$ value for CA(1−7)M(2−9) is higher than the ones for the methylated derivatives (although of the same order of magnitude).

Regarding the saturation process, Melo et al. suggest the existence of membrane-bound peptide concentrations at which the outer leaflet of the membrane is essentially saturated, whereas the inner leaflet still remains free of peptide.[53]As a result, the overall mechanism would involve the initial adsorption of the peptide at the membrane interface, with segregation of negative lipids (PG) from zwitterionic ones, followed by some conformation/localization change under saturation that accounts for the increase in its fluorescence quantum yield.

POPE:POPG (3:1) Model Membranes. The partition of CA(1−7)M(2−9) and its trimethylated derivatives K6 and K7 was also studied for the POPE:POPG (3:1) lipid system. The preliminary steady-state fluorescence experiments revealed that the samples had undergone extensive flocculation, causing a partial sedimentation of the lipid−peptide aggregates, even at low lipid concentration (350 μM), compromising the analysis of the steady-state data. Therefore, this system was studied by TRFS.

The fluorescence intensity decay curves for the three peptides CA(1−7M(2−9), K6, and K7 in buffer and upon partitioning to the POPE:POPG (3:1) lipid membrane were fitted by a sum of three discrete exponentials (eqs 1 and 2), from which the lifetime-weighted quantum yield ($\bar{\tau}$) was calculated. Figure 4 shows a plot of the lifetime-weighted quantum yield ($\bar{\tau}$) as a function of lipid concentration (outer leaflet) for the three peptides. It can be seen that the interaction of the peptides with POPE:POPG 3:1 lipid vesicles caused a progressive increase in their lifetime-weighted quantum yield, revealing their incorporation in a more hydrophobic environment. The partition constant was obtained from nonlinear fitting of eq 6 to the obtained data, and the parameters retrieved, $K_{p,x}$ and $\bar{\tau}_L$, for CA(1−7)M(2−9), K6, and K7 peptides are displayed in Table 4.

It can be observed that CA(1−7)M(2−9) has a higher partition constant than the ones obtained for the trimethylated versions, which are the same within uncertainty limits, indicating that *N*-trimethylation slightly decreases the extent of partition to this lipid membrane. This trend is in line with the previous observations for the DMPC:DMPG system.

Concerning the fluorescence anisotropy results (Figure 5), the increase of the steady-state anisotropy upon binding to the membrane is similar both for methylated peptides ($\langle r \rangle_L \cong 0.119$ and $\langle r \rangle_L = 0.136$, for K6 and K7, respectively) and for the

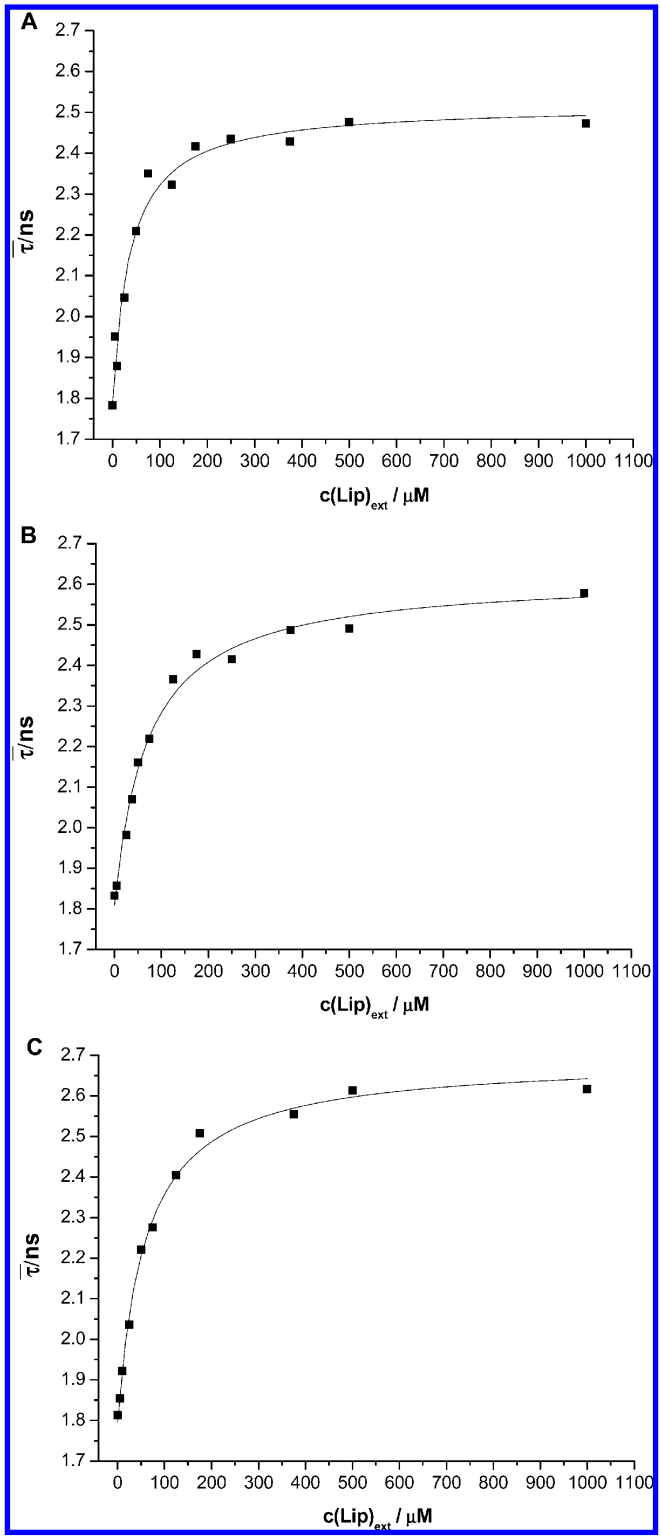

Figure 4. Lifetime-weighted quantum yield, $\bar{\tau}$, as a function of the lipid concentration (outer leaflet) for the POPE:POPG (3:1) system at 30 °C. The symbol (■) represents the experimental values and the line corresponds to the fitted curve according to eq 6 for the parental peptide CA(1−7)M(2−9) (A) and the trimethylated derivatives K6 (B) and K7 (C).

parental peptide ($\langle r \rangle_L = 0.127$). This allows us to conclude that the tryptophan residue locates in a more ordered environment, probably confined at the phospholipid−water interface by electrostatic interaction with the anionic phospholipids, consistent with lipid phase segregation, as demonstrated by DSC

TABLE 4: Partition Coefficients ($K_{p,x}$) for the Interaction of the Parental Peptide CA(1−7)M(2−9) and the Trimethylated Derivatives K6 and K7 with the Lipid System POPE:POPG (3:1), As Obtained by TRFS

peptide	$K_{p,x}$	$\bar{\tau}_L$/ns
CA(1−7)M(2−9)	$(1.5 \pm 0.4) \times 10^6$	2.52 ± 0.03
K6	$(7.5 \pm 0.9) \times 10^5$	2.65 ± 0.03
K7	$(9.4 \pm 1.0) \times 10^5$	2.69 ± 0.02

results. This increase in anisotropy happens even considering the fact that the fluorescence lifetime increases, providing further evidence for a restricted dynamics of the residue.

Time-resolved fluorescence anisotropy decay measurements were also carried out to obtain a more detailed view about the rotational and segmental dynamics of the tryptophan residues in the K6 and K7 peptides (Table 5).

Both K6 and K7 peptides display two rotational correlation times in aqueous solution, a long one (φ_2) of ∼0.4−0.5 ns and a very short one (φ_1) of ∼40−50 ps, each component contributing about equally to the total observable decay in anisotropy. In both cases, the initial anisotropy is $r(0) \sim 0.28-0.29$, very close to the expected value of 0.3. Since the long rotational correlation time (φ_2) is 8−13-fold the short one (φ_1), the total anisotropy can be described as the result of two independent depolarizing events:[54]

$$r(t) = r'(t)e^{-t/\varphi_{global}} \quad (8A)$$

$$r'(t) = r(0)[(1 - S_1^2)e^{t/\varphi_{segmental}} + S_1^2] \quad (8B)$$

In this case, the kinetics of the decay is a combination of the [$r(t)$] term (eq 8A), describing the global tumbling motion of the whole peptide in solution and a [$r'(t)$] term attributed to local fast movements of the peptide's segment containing the tryptophan residue (eq 8B). The S_1 parameter is the order parameter that characterizes the internal fluctuations of the peptide segment containing the tryptophan.

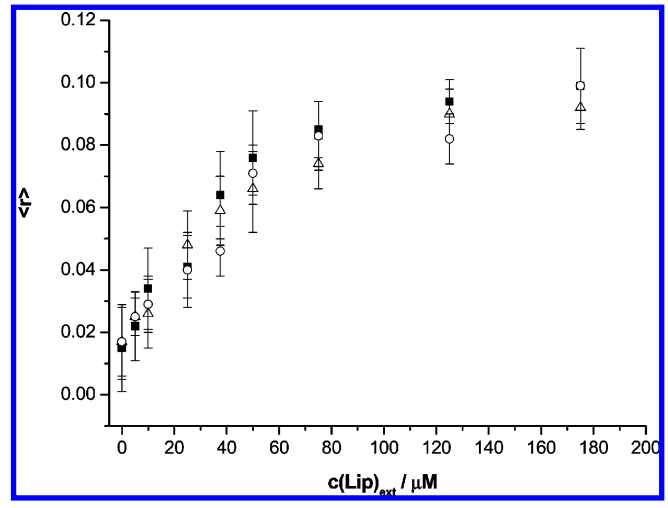

Figure 5. Steady-state anisotropy of tryptophan as a function of the lipid concentration (outer leaflet) for the POPE:POPG (3:1) system at 30 °C. The symbol represents the experimental values, and the bars respresent the corresponding error ranges, for the parental peptide CA(1−7)M(2−9) (■) and the trimethylated derivatives K6 (Δ) and K7 (O). Excitation and emission wavelengths were 282 and 350 nm, respectively.

TABLE 5: Time-Resolved Fluorescence Anisotropy Parameters for CA(1−7)M(2−9) and the Trimethylated Analogues K6 and K7 (Rotational Correlation Times, φ_i, Segmental and Global Correlation Times, $\varphi_{segmental}$ and φ_{global}, Amplitudes, β_i, and Residual Anisotropy, r_∞, and Quality of the Fit, χ^2) in Aqueous Buffer and with POPE:POPG (3:1) LUVs (175 μM, Outer Leaflet Concentration) at 30 °C

medium	peptide	$r(0)$	β_1	φ_1 (ns)	β_2	φ_2 (ns)	$\varphi_{segmental}$ (ns)	φ_{global} (ns)	r_∞	χ^2
buffer	K6	0.29	0.17	0.043	0.12	0.54	0.05	0.54		1.19
	K7	0.28	0.14	0.048	0.14	0.37	0.06	0.37		1.14
lipid	K6	0.16			0.07	2.4			0.09	1.17
	K7	0.16			0.05	2.6			0.11	1.18

TABLE 6: Parameters from the Fit of an Independent Two-Motion Model to the Anisotropy Decay of the Trimethylated Analogues K6 and K7 (Order Parameters, S_i, and Cone Angles, θ_i) in Aqueous Buffer and with POPE:POPG (3:1) LUVs (175 μM, Outer Leaflet Concentration) at 30 °C

medium	peptide	S_1	θ_1 (deg)	S_2	θ_2 (deg)
buffer	K6	0.64	43		
	K7	0.71	38		
lipid	K6			0.76	34
	K7			0.82	29

The two rotational correlation times (φ_1 and φ_2) are related to φ_{global} and $\varphi_{segmental}$ by eqs 9A-9B:

$$\varphi_2 = \varphi_{global} \tag{9A}$$

$$\varphi_1 = \frac{\varphi_{segmental}\varphi_{global}}{\varphi_{segmental} + \varphi_{global}} \tag{9B}$$

The very fast motions as well as the internal conversion between the ^1L_a and ^1L_b states of tryptophan cannot be resolved by our system, which has a response time in the range of 30 ps. The order parameters S_1 values obtained using eq 8B are shown in Table 6. The angular displacement of these movements can be obtained from the order parameter S_1 assuming a "wobbling-in-cone" model. According to this model, the cone angle θ in which the rotation of the peptide segment containing the tryptophan residue occurs is given by the eq 10:

$$\cos\theta = \frac{1}{2}[\sqrt{(8S_1 + 1)} - 1] \tag{10}$$

Cone angles of rotation of 43° and 38° were obtained for K6 and K7, confirming that the tryptophan-containing peptide segment experiences large angular displacements during its fluorescence lifetime. Such angular displacements are expected considering the random coil conformation adopted by both peptides in solution, which must confer a high flexibility to the tryptophan-containing peptide segment. Since the long correlation time (φ_2) is directly related to φ_{global} and no significant difference in the values for the two peptides is observed, the global rotational motion is similar for both peptides.

Upon partitioning to the lipid membrane, the anisotropy decays for both peptides presented similar kinetics (similar φ_2 values) reaching a residual, time-independent value, different from zero, $r_\infty \sim 0.09-0.11$, in contrast to the anisotropy profiles measured in buffer. In this case, only one long rotational correlation time $\varphi_2 \sim 2.4-2.6$ ns was sufficient to adequately describe the fluorescence anisotropy curves. In addition, the $r(0)$ values were much lower than the value ~0.30 value expected for an immobilized tryptophan residue upon excitation at 300 nm. This result strongly suggests that an ultrafast energy homotransfer between tryptophan residues of different peptides may be taking place, probably resulting from the high peptide surface concentration at the membrane level in the liposomes. This is compatible with the charge clustering and lipid phase segregation as proposed by Epand et al.,[47] which highly confines the peptide locally at the membrane level due to preferential binding to the anionic phospholipids and sternly limits the movement of the whole peptide after insertion to the aliphatic region of the lipid vesicle.[11]

The residual anisotropy value, r_∞, is indicative of an energetic barrier that restricts the rotational diffusion of the tryptophan residue on the time scale of the experiment. Following the model previously used for the anisotropy experiments in solution, the total anisotropy was interpreted as resulting only from the global rotational motion of the whole peptide partitioned into the lipid bilayer:[54]

$$r'(t) = r(0)[(1 - S_2^2)e^{-t/\varphi_2} + S_1^2] \tag{11}$$

The cone angles of rotation of the membrane-interacting peptides K6 and K7, calculated using the values of $S_2^2 = r_\infty/r(0)$, are 34° and 29°, respectively (Table 6).

This shows that the membrane-bound peptide segment experiences smaller angular displacements during its tryptophan lifetime than the free peptide in solution. Such small angular displacements are expected considering the low flexibility of the peptide segment after acquiring a secondary structure (α-helix) upon the initial adsorption to the water-membrane interface, as shown by NMR measurements.[40]

Discussion

The influence of peptide properties and the membrane composition on the mechanism of action of AMPs are both vital to understanding the modulation of membrane dynamics (shape, phase, membrane pressure profile, curvature strain) by peptides, and to possibly infer consequences on cellular metabolism and viability.

Taken together, the present DSC and fluorescence spectroscopy data provide evidence for a different interaction profile of modified K6 and K7 peptides as compared to that of CA(1−7)M(2−9) depending on the model system used, showing that the peptide's activity is influenced by the lipid composition.[49,55]

Our fluorescence results show that N^ε-trimethylation slightly decreased the magnitude of partition of the trimethylated peptides to DMPC:DMPG vesicles as compared to the magnitude of partition of the parental peptide and that a different threshold was found for these derivatives than for CA(1−7)M(2−9)[42] in this model membrane system, which may derive from the different partition constant of the peptides. In fact, CA(1−7)M(2−9) presents a higher partition constant; therefore, a lower peptide concentration is needed to achieve membrane saturation (1:12) as compared to case for the methylated derivatives (1:9). The DSC results, on the other hand,

indicate that subtle differences can be observed within the same model system, depending on the peptide. In particular, DSC shows that for K7, lipid phase segregation is already apparent at 1:80, even before the membrane saturation threshold, whereas for K6 a peptide-to-lipid ratio of 1:15 is required. Furthermore, the dramatic decrease in the transition enthalpy observed for K7 (P:L = 1:15) suggests that this peptide induces more extensive perturbation on the hydrophobic core and that the interaction is somehow improved compared to the case for K6. This difference may be due to a more pronounced internalization of the K7 peptide into the hydrophobic core of the membrane, probably arising from particular conformational constraints upon N^{ε}-trimethylation at this position. On the other hand, CA(1−7)-M(2−9) does not promote substantial lipid demixing at the highest P:L,[41] indicating that we are in the presence of a different mechanism of action. In fact, the ability of CA(1−7)M(2−9) to partition to both PC and PG justifies the higher partition constant estimated for this peptide. Altogether, the present data appear to favor pore formation for the parental peptide, probably of the toroidal type, at high peptide concentrations, as proposed by Bastos et al.[42] and Milani et al.[56] The trimethylated derivatives K6 and K7, on the other hand, do not partition to PC, according to our steady-state fluorescence spectroscopy results and must therefore explore another mechanistic process. According to the DSC results, we propose that the mechanism of lipid clustering of anionic phospholipids (PG) from zwitterionic ones (PC) induced by AMPs is the basis of the observed behavior of the trimethylated analogues.

As for the other membrane-mimetic system, POPE:POPG, the DSC results show that CA(1−7)M(2−9) stabilizes the membrane at low P:L ratios, as previously discussed, but at the intermediate P:L (1:40), there is an asymmetric thermogram characterized by the existence of two DSC peaks, consistent with the formation of two different domains with distinct lipid and peptide composition. However, at the highest P:L (1:15), a significant decrease in the transition enthalpy is observed and the peak splitting is no longer observed. At this P:L ratio, it is expected that the peptide has inserted into the membrane to form pores due to its ability to also interact with zwitterionic lipids.[41] In addition, a higher $K_{p,x}$ value is obtained for CA(1−7)M(2−9) from TRFS results, corroborating a higher membrane destabilization for this peptide at the highest P:L ratio. The trimethylated peptides induce a large asymmetry of the DSC peak, more consistent with the lipid segregation mechanism than with pore formation. The final location of both peptides in the membrane is expected to be similar, since comparable steady-state anisotropy values were obtained in each case. At this point, K7 appears to induce a more significant perturbation, which is consistent with the absence of the stabilizing effect at 1:80 P:L ratio and a slightly higher partition constant than K6. As a result, we suggest that also for this model membrane system, the main mechanism of CA(1−7)M(2−9) is initially a modest lipid segregation followed by pore formation at high peptide concentration whereas the trimethylated derivatives may proceed by lipid segregation into different peptide−lipid domains, albeit with a more pronounced effect than observed on PC:PG system.

The evaluation of the hemolytic profile of the trimethylated peptides was performed using DMPC as a model membrane. The steady-state fluorescence data show that the modified versions do not partition to the DMPC membrane, even at high lipid concentration (4 mM) (data not shown). Fernández-Reyes et al.[40] point out that the increase in bulkiness of the ε-NH_2 group of the side chain of Lys residues due to the addition of methyl groups creates important stereochemical and orientational constraints that attenuate the interaction with the polar headgroups of the phospholipids. We further propose that the methyl groups, as electronic donor groups, decrease the magnitude of the intrinsic positive charge of Lys, thus contributing to the observed decay in cytotoxicity. Recent studies have shown that high amphipathicity, high hydrophobicity and as high helicity or β-sheet structure directly correlated with increased cytotoxicity.[57−59] The same group has also highlighted the impact of hydrophobicity on the partition process[40] as their analytical RP-HPLC results have shown that all methylated derivatives have a lower hydrophobicity as compared to the parental peptide CA(1−7)M(2−9) results, consistent with the observed decrease on hemolytic activity and absence of and membrane partition to the DMPC model membrane system used here.

Some studies have also shown that hemolytic activity depends not only on the net charge of the peptide (electrostatic interactions) but also on the formation of hydrogen bonds with both carbonyl and phosphate groups of the phospholipids.[50,60] In the present case, the N-trimethylation of the ε-amino group of Lys residues is accompanied by a loss of hydrogen bond potential, which may abrogate the interaction with the PC model membrane, an effect already observed by Kandasamy et al.[60]

In general, our results display the same trends observed by Fernández-Reyes et al.,[40] showing a very good correlation between the thermodynamics of the peptide/membrane interaction and the clear drop of the hemolytic activity for K6 and K7 trimethylated derivatives as compared to that for CA(1−7)M(2−9).

The minimal inhibitory concentration (MIC_{50}) against *A. baumannii* is slightly smaller for the parental peptides than for the trimethylated derivatives, although the values cross on the limits of the confidence intervals, indicating that no strikingly significant activity differences were found among the three peptides against this bacterium. Our results are in agreement with this study as although the obtained $K_{p,x}$ values for DMPC:DMPG are of the same order of magnitude, a higher value was estimated for the parental peptide, and a similar trend is observed for POPE:POPG. Regarding Gram-positive bacteria, the MIC_{50} value for CA(1−7)M(2−9) in *S. aureus* is clearly lower for this peptide, and accordingly our partition constant ($K_{p,x}$) is higher than those observed for K6 and K7 peptides. Even for *L. donovani* promastigotes and *L. pifanoi* amastigotes, the same tendency is observed. However, it is important to recognize that this system is not the most appropriated one for *S. aureus* since this bacterium is mostly composed of anionic phospholipids [PG and cardiolipin (CL)]. Moreover, *Leishmania* is a genus of trypanosome protozoa with a very complex lipid and protein composition that clearly limits the application of this model membrane system as a suitable mimetic system.

Therefore, overall, the results show a good agreement between the microbiology and our biophysical results, indicating that such biophysical studies are a very promising road on the unraveling of activity of AMPs.

Conclusions

The aim of this work was to study the effect of N^{ε}-trimethylation at different positions on the activity of CA(1−7)-M(2−9) on membrane-mimetic lipid systems of different composition, in an effort to understand the contribution of trimethylation to a more selective mechanism of action. For this purpose, DSC and fluorescence spectroscopy were used to evaluate the influence of the peptides on the thermotropic phase transition of DMPC:DMPG, POPE:POPG mixed vesicles at different P:L ratios, and to characterize the partition of peptides in model membrane systems.

The trimethylated derivatives K6 and K7 were chosen for the present study as they had shown a significant improvement in selectivity toward microbial (vs eukaryotic) target cells.[40] Our results clearly show that these peptides retain the ability to strongly interact with partially negatively charged membranes (DMPC:DMPG and POPE:POPG) and that the process is driven by the electrostatic interaction between the charged peptide and the anionic phospholipids of the bilayer, whereas they do not interact significantly with DMPC membranes, in contrast with the parental peptide.[41,42] This clearly indicates the importance of electrostatics on the initial approach of the peptide to the membrane and on the overall partition process. The effect of N^{ε}-trimethylation on MIC_{50} values for the Gram-negative bacterium is consistent with our results.[40] We demonstrate here that partition studies are very important for obtaining correlations with biological activity (MIC), and that DSC studies further show that the detailed mechanism depends both on peptide chemical structure and lipid composition of the membrane system.

To explain the considerable decrease of the hemolytic character of the trimethylated analogues,[40] it was proposed that stereochemical constraints introduced by the bulkiness of the trimethylated ε-amino group of the Lys residue are the main factor responsible for the decrease in interaction with the phospholipids' headgroups.

We found that a mechanistic difference probably exists between the trimethylated peptides and the parental CA(1−7)-M(2−9), as we propose that the last one may act through a dual mechanism of initial and partial phospholipid domain segregation, followed by pore formation, as revealed by DSC, due to its capacity to partition to both anionic and zwitterionic membranes. The trimethylated peptides K6 and K7, on the other hand, would act mainly through a segregation mechanism in both lipid systems.

Acknowledgment. Thanks are due to FCT for financial support to CIQ(UP), Unidade de Investigação 81 and to CRUP and MICINN for financial support of a Portuguese/Spanish integrated Action (E40/09). Work in Spain was supported by the European Union (HEALTH-2007-223414, *Leishdrug*, to L.R. and D.A.), the Spanish Ministry of Science and Innovation (PET2006-0139 to D.A. and L.R., BIO2005-07592-CO2-02 and BIO200804487-CO3-02 to D.A.), Fondo de Investigaciones Sanitarias (PI061125, PS09-01928, and RD06/0021/0006 to L.R., PI040885 to D.A.), and by the regional governments of Madrid (S-BIO-0260/2006 to L.R.) and Catalonia (SGR2005-00494).

References and Notes

(1) Meincken, M.; Holroyd, D. L.; Rautenbach, M. *Antimicrob. Agents Chemother.* **2005**, *49*, 4085.
(2) Basselin, M.; Robert-Gero, M. *Parasitol. Res.* **1998**, *84*, 78.
(3) Watson, J. L.; Gillies, E. R. *J. Org. Chem.* **2009**, *74*, 5953.
(4) Lata, S.; Sharma, B.; Raghava, G. *BMC Bioinf.* **2007**, *8*, 263.
(5) Shin, S. Y.; Yang, S.-T.; Park, E. J.; Eom, S. H.; Song, W. K.; Kim, J. I.; Lee, S.-H.; Lee, M. K.; Lee, D. G.; Hahm, K.-S.; Kim, Y. *J. Peptide Res.* **2001**, *58*, 504.
(6) Li, A.; Lee, P. Y.; Ho, B.; Ding, J. L.; Lim, C. T. *Biochim. Biophys. Acta, Biomembr.* **2007**, *1768*, 411.
(7) Glukhov, E.; Stark, M.; Burrows, L. L.; Deber, C. M. *J. Biol. Chem.* **2005**, *280*, 33960.
(8) Jiang, Z.; Vasil, A. I.; Hale, J. D.; Hancock, R. E. W.; Vasil, M. L.; Hodges, R. S. *Pept. Sci.* **2008**, *90*, 369.
(9) Chan, D. I.; Prenner, E. J.; Vogel, H. J. *Biochim. Biophys. Acta, Biomembr.s* **2006**, *1758*, 1184.
(10) Dawn, M. E. B.; Donald, J. D.; Robert, E. W. H. *Curr. Protein Pept. Sci.* **2005**, *6*, 35.
(11) Huang, H. W. *Biochemistry* **2000**, *39*, 8347.
(12) Stella, L.; Mazzuca, C.; Venanzi, M.; Palleschi, A.; Didonè, M.; Formaggio, F.; Toniolo, C.; Pispisa, B. *Biophys. J.* **2004**, *86*, 936.
(13) Jeong, K.-W.; Shin, S.; Kim, J.-K.; Kim, Y. *Bull. Korean Chem. Soc.* **2009**, *30*, 1839.
(14) Wachinger, M.; Kleinschmidt, A.; Winder, D.; von Pechmann, N.; Ludvigsen, A.; Neumann, M.; Holle, R.; Salmons, B.; Erfle, V.; Brack-Werner, R. *J. Gen. Virol.* **1998**, *79*, 731.
(15) Papo, N.; Shai, Y. *Peptides* **2003**, *24*, 1693.
(16) Sood, R.; Kinnunen, P. K. J. *Biochim. Biophys. Acta, Biomembr.* **2008**, *1778*, 1460.
(17) Zhao, H.; Mattila, J.-P.; Holopainen, J. M.; Kinnunen, P. K. J. *Biophys. J.* **2001**, *81*, 2979.
(18) Easton, D. M.; Nijnik, A.; Mayer, M. L.; Hancock, R. E. W. *Trends Biotechnol.* **2009**, *27*, 582.
(19) Hancock, R. *Lancet Infect. Dis.* **2001**, *1*, 156.
(20) Yount, N. Y.; Bayer, A. S.; Xiong, Y. Q.; Yeaman, M. R. *Pept. Sci.* **2006**, *84*, 435.
(21) Jenssen, H.; Hamill, P.; Hancock, R. E. W. *Clin. Microbiol. Rev.* **2006**, *19*, 491.
(22) Mahalka, A. K.; Kinnunen, P. K. J. *Biochim. Biophys. Acta, Biomembr.* **2009**, *1788*, 1600.
(23) Auvynet, C.; El Amri, C.; Lacombe, C.; Bruston, F.; Bourdais, J.; Nicolas, P.; Rosenstein, Y. *FEBS J.* **2008**, *275*, 4134.
(24) Soscia, S. J.; Kirby, J. E.; Washicosky, K. J.; Tucker, S. M.; Ingelsson, M.; Hyman, B.; Burton, M. A.; Goldstein, L. E.; Duong, S.; Tanzi, R. E.; Moir, R. D. *PLoS ONE* **2010**, *5*, e9505.
(25) Pasupuleti, M.; Roupe, M.; Rydengård, V.; Surewicz, K.; Surewicz, W. K.; Chalupka, A.; Malmsten, M.; Sörensen, O. E.; Schmidtchen, A. *PLoS ONE* **2009**, *4*, e7358.
(26) Epand, R. F.; Wang, G.; Berno, B.; Epand, R. M. *Antimicrob. Agents Chemother.* **2009**, *53*, 3705.
(27) Zweytick, D.; Tumer, S.; Blondelle, S. E.; Lohner, K. *Biochem. Biophys. Res. Commun.* **2008**, *369*, 395.
(28) Haney, E. F.; Nathoo, S.; Vogel, H. J.; Prenner, E. J. *Chem. Phys. Lipids* **2010**, *163*, 82.
(29) Mochon, A. B.; Liu, H. *PLoS Pathog.* **2008**, *4*, 1.
(30) Epand, R. M.; Epand, R. F. *Biochim. Biophys. Acta, Biomembr.* **2009**, *1788*, 289.
(31) Yeaman, M. R.; Yount, N. Y. *Pharmacol. Rev.* **2003**, *55*, 27.
(32) Rosenfeld, Y.; Lev, N.; Shai, Y. *Biochemistry* **2010**, *49*, 853.
(33) Andreu, D.; Ubach, J.; Boman, A.; Wåhlin, B.; Wade, D.; Merrifield, R. B.; Boman, H. G. *FEBS Lett.* **1992**, *296*, 190.
(34) Chicharro, C.; Granata, C.; Lozano, R.; Andreu, D.; Rivas, L. *Antimicrob. Agents Chemother.* **2001**, *45*, 2441.
(35) Mathur, P.; Jagannathan, N. R.; Chauhan, V. S. *J. Pept. Sci.* **2007**, *13*, 253.
(36) Sato, H.; Feix, J. B. *Antimicrob. Agents Chemother.* **2008**, *52*, 4463.
(37) Shin, S. Y.; Kang, J. H.; Lee, D. G.; Jang, S. Y.; Seo, M. Y.; Kim, K. L.; Hahm, K.-S. *Bull. Korean Chem. Soc.* **1999**, *20*, 1078.
(38) Chatterjee, J.; Gilon, C.; Hoffman, A.; Kessler, H. *Acc. Chem. Res.* **2008**, *41*, 1331.
(39) Biron, E.; Chatterjee, J.; Ovadia, O.; Langenegger, D.; Brueggen, J.; Hoyer, D.; Schmid, Herbert, A.; Jelinek, R.; Gilon, C.; Hoffman, A.; Kessler, H. *Angew. Chem., Int. Ed.* **2008**, *47*, 2595.
(40) Fernández-Reyes, M.; Díaz, D.; de la Torre, B. G.; Ania Cabrales-Rico, A.; Vallès-Miret, M.; Jiménez-Barbero, J.; Andreu, D.; Rivas, L. *J. Med. Chem.* 2010.
(41) Abrunhosa, F.; Faria, S.; Gomes, P.; Tomaz, I.; Pessoa, J. C.; Andreu, D.; Bastos, M. *J. Phys. Chem. B* **2005**, *109*, 17311.
(42) Bastos, M.; Bai, G.; Gomes, P.; Andreu, D.; Goormaghtigh, E.; Prieto, M. *Biophys. J.* **2008**, *94*, 2128.
(43) Pistolesi, S.; Pogni, R.; Feix, J. B. *Biophys. J.* **2007**, *93*, 1651.
(44) Poveda, J. A.; Prieto, M.; Encinar, J. A.; Gonzalez-Ros, J. M.; Mateo, C. R. *Biochemistry* **2003**, *42*, 7124.
(45) Valeur, B.; Weber, G. *Photochem. Photobiol.* **1977**, *25*, 441.
(46) Santos, N. C.; Prieto, M.; Castanho, M. A. R. B. *Biochim. Biophys. Acta, Biomembranes* **2003**, *1612*, 123.
(47) Epand, R. F.; Maloy, W. L.; Ramamoorthy, A.; Epand, R. M. *Biochemistry* **2010**, *49*, 4076.
(48) Epand, R. M. *Biophys. Chem.* **2007**, *126*, 197.
(49) Arouri, A.; Dathe, M.; Blume, A. *Biochim. Biophys. Acta, Biomembranes* **2008**, *1788*, 650.
(50) Yamamoto, N.; Tamura, A. *Peptides* **2010**, *5*, 794.
(51) Pozo Navas, B.; Lohner, K.; Deutsch, G.; Sevcsik, E.; Riske, K. A.; Dimova, R.; Garidel, P.; Pabst, G. *Biochim. Biophys. Acta, Biomembranes* **2005**, *1716*, 40.
(52) Schwieger, C.; Blume, A. *Eur. Biophys. J.* **2007**, *36*, 437.
(53) Melo, M. N.; Castanho, M. A. R. B. *Biochim. Biophys. Acta, Biomembranes* **2007**, *1768*, 1277.
(54) Lipari, G.; Szabo, A. *Biophys. J.* **1980**, *30*, 489.
(55) Lohner, K.; Sevcsik, E.; Pabst, G. *Adv. Planar Lipid Bilayers Liposomes* **2008**, *6*, 103.

(56) Milani, A.; Benedusi, M.; Aquila, M.; Rispoli, G. *Molecules* **2009**, *14*, 5179.

(57) Takahashi, D.; Shukla, S. K.; Prakash, O.; Zhang, G. *Biochimie* 2010.

(58) Chen, Y.; Guarnieri, M. T.; Vasil, A. I.; Vasil, M. L.; Mant, C. T.; Hodges, R. S. *Antimicrob. Agents Chemother.* **2007**, *51*, 1398.

(59) Chen, Y.; Mant, C. T.; Farmer, S. W.; Hancock, R. E. W.; Vasil, M. L.; Hodges, R. S. *J. Biol. Chem.* **2005**, *280*, 12316.

(60) Kandasamy, S. K.; Larson, R. G. *Chem. Phys. Lipids* **2004**, *132*, 113.

JP106915C